Comprehensive Digital Correction of Mismatch Errors for a 400-Msamples/s 80-dB SFDR Time-Interleaved Analog-to-Digital Converter

Munkyo Seo, Mark J. W. Rodwell, *Fellow, IEEE*, and Upamanyu Madhow, *Senior Member, IEEE*

***Abstract*—Comprehensive digital calibration of a high-speed and high-resolution time-interleaved analog-to-digital converter (TIADC) is described. A channel transfer function, which incorporates all linear errors between analog input and digital output, is measured for each channel by applying a series of sinusoids. A set of finite-impulse response (FIR) filters designed by the weighted least squares principle provides frequency-dependent mismatch correction so that the spurious-free dynamic range (SFDR) is no longer limited by channel mismatches. A four-channel TIADC prototype with 14-bit resolution and 400-MHz aggregate sampling rate was built to verify the proposed correction method. Uncalibrated SFDR was below 50 dB. After mismatch correction with 61-tap FIR filters, 80 dB of SFDR was achieved up to ∼175 MHz of input frequency.**

***Index Terms*—Analog–digital conversion, calibration, mismatch correction, time-interleaved analog-to-digital converters (TIADCs).**

I. Introduction

In order to increase the sampling rate of an analog-to-digital converter (ADC) beyond a certain process technology limit, the use of a time-interleaved analog-to-digital converter (TIADC) has been proposed [1]–[20], [27]–[29]. A TIADC has a parallel structure where a number of ADCs independently sample the input signal. The input analog signal is successively sampled by each ADC in a cyclic manner, and the digital output is similarly taken from each ADC to reconstruct the signal stream in digital form. The overall sampling rate is, therefore, multiplied by the number of ADCs. A TIADC finds its application in electronic systems such as radar, direct digital receivers, base-station receivers, and high-speed instrumentation, as well as opto-electric systems including photonic ADCs [4]–[7].

A TIADC performs high-throughput analog-to-digital (A/D) conversion with no degradation in spectral purity if all ADCs have identical electrical characteristics (e.g., gain, sampling time, input bandwidth, dc offset, etc.). In practice, however, various electrical mismatches are inevitable, which periodically modulate the input signal. The array's spurious-free dynamic range (SFDR) is then reduced due to spurious sidebands generated by this modulation.

Manuscript received September 2, 2004; revised November 24, 2004. This work was supported by the Office of Naval Research under Grant N000140410104 and by the Graduate Division, University of California at Santa Barbara under a Science and Engineering Research Grant.

The authors are with the Department of Electrical and Computer Engineering, University of California at Santa Barbara, CA 93106 USA (e-mail: mkseo@engineering.ucsb.edu).

Digital Object Identifier 10.1109/TMTT.2005.843487

Therefore, to achieve the highest SFDR feasible, channel mismatches must be eliminated or calibrated by using either analog circuitry [8], [9], [11]–[13] or digital signal processing [14]–[20]. Digital correction is preferred due to its reliability and flexibility. Continued scaling of process technologies also make digital processing increasingly inexpensive.

Traditionally, TIADC mismatch correction has been mostly attempted in terms of several frequency-independent parameters such as gain, sampling time, and offset mismatches. This parametric approach is easily implemented, and is adequate for low-to-moderate resolutions. In high-resolution data conversion, however, spectral purity is easily compromised by even slight channel mismatches because of the low quantization noise floor. For example, 80 dB of SFDR requires approximately 0.01% of residual channel mismatches [7]. Parametric correction is, in general, not able to achieve this level of mismatch correction over a wide frequency range and, therefore, comprehensive (i.e., frequency dependent) mismatch correction is necessary. Very high-speed time-interleaved A/D conversion may also require comprehensive mismatch correction due to differences between channels in the high-frequency transfer functions of the input analog circuitry.

The application of hybrid filter banks (HFBs) to TIADC has been proposed to attenuate channel mismatches [21]–[23], [25]. In this architecture, a set of analog filters split the input signal into separate frequency bands in either discrete [21] or continuous [22], [23], [25] time. Outputs from sub-converters are combined through a digital filter bank. Although the performance of HFB converters is less sensitive to mismatch errors than conventional TIADCs, the need of accurate analog filters restricts their practical use.

Recently, an important observation has been made by Velazquez and Velazquez [24]: *analog filters at the input are not necessary given a properly designed digital filter bank*. This suggests a practical way of mismatch correction for high-performance TIADCs, i.e., comprehensive error correction only by digital post-processing. Commercial TIADC products, with 12-bit resolution and 400–500 Msamples/s (MSPS) conversion rate, are also developed based on his approach [35], [36].

In this paper, we propose a comprehensive mismatch correction method, as well as experimental verification, which, unlike the previous techniques, fully exploits the stopband structure of input analog circuitry for more efficient correction. In designing correction finite-impulse response (FIR) filters, aliasing spurs due to the sub-converter mismatches are individually controlled within the computational framework of the weighted least squares (WLSs).

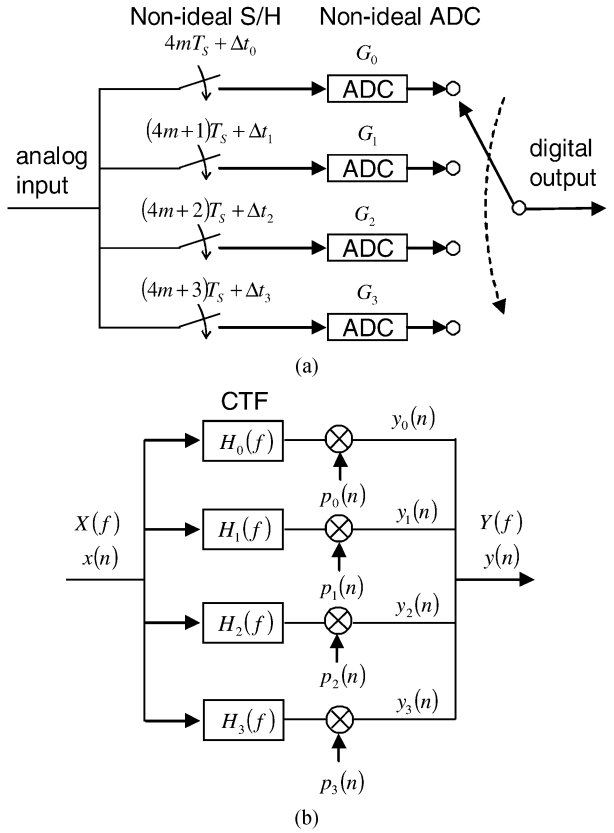

Fig. 1. Four-channel time-interleaved ADC system. (a) Actual system with two representative linear imperfections (i.e., unequal sampling time deviation and ADC gain). (b) General linear model with CTFs. An output multiplexing switch in (a) is replaced by a multiplication by an impulse train. All the linear distortions in each channel are lumped into a single CTF.

A frequency-dependent linear model of the TIADC is derived in Section II. Section III describes generation of aliasing errors in terms of the linear model. In Section IV, the characterization of channel mismatches is discussed along with practical concerns. Sections V and VI each presents the design of FIR filters and experimental results of a 14-bit 400-MSPS prototype. Section VII gives the conclusion.

II. Linear Model of TIADC

Fig. 1(a) shows a four-channel TIADC configuration. Each channel converts analog input signal every $4T_S$ with an appropriate delay so that the aggregate sampling rate is $f_S(=1/T_S)$. The bandwidth of the input signal has to be smaller than $f_S/2$ to avoid aliasing. Although operation in any Nyquist zone is possible as long as the sample-and-hold (S/H) circuitry has sufficient bandwidth, we assume, for simplicity, that the input signal is confined within the first Nyquist zone, i.e., from dc to $f_S/2$. It is noted that, for M-channel interleaved operation, the S/H blocks must have M-times wider bandwidth than is required for single-channel conversion at f_S/M, i.e., their input bandwidth has to be equal to or greater than $f_S/2$. M-channel interleaved A/D conversion also requires the sampling clock to have M-fold higher timing stability (lower phase noise).

The assumption of a band-limited input simplifies notation by allowing discrete-time representation of all signals including the ADC input. Although $H(e^{j2\pi fT_S})$ is the conventional notation for a discrete-time frequency spectrum with period f_S, we instead use $H(f)$ throughout the paper for readability.

All S/H and ADC blocks are assumed to be linear and have zero offset. Channel offset is independently measured during calibration and is subsequently digitally subtracted from each ADC output. Time invariance (or shift invariance) is assumed for all linear systems. Assuming that the resolution of the individual ADCs is high, we neglect their quantization effects.

In Fig. 1(a), two typical sources of mismatches are shown: G_k's and Δt_k's for A/D conversion gain and systematic sampling time deviation from a nominal point, respectively. As we will show later with experimental data, G_k and Δt_k are not sufficient to describe all significant TIADC errors. For example, S/H blocks may have different 3-dB bandwidth, and the adjacent channels may have unequal crosstalk due to the integrated-circuit (IC) interconnect environment or due to a finite S/H off-state isolation. Small variations will exist between channels in their midband frequency response due to power supply and ground impedance and standing waves on interconnects.

A TIADC system with all these linear imperfections can be conveniently modeled with a set of equivalent channel-transfer functions (CTFs) followed by a multiplication by an impulse train, as can be seen in Fig. 1(b)

$$p_k(n)=\sum_{m=-\infty}^{\infty}\delta\big(n-(mM+k)\big),\qquad k=0,1,\ldots,M-1$$

whose period is equal to M, the number of TIADC channels. $\delta(n)$ is the delta function. For example, with only gain and timing error, a CTF will have the form $H_k(f)=G_k e^{-j2\pi f\Delta t_k}$. A CTF may actually include *any linear* distortion pertaining to each channel from S/H input to ADC output. It may also incorporate preceding linear systems common to all channels (e.g., an antialiasing filter). It is noted that CTFs are not necessarily causal, especially when there is a sampling time mismatch. This comes from the fact that a band-limited signal at any instance can be represented as a weighted sum of nominal sample values, both in the past and future [26].

III. Generation of Aliasing Error

Aliasing in the presence of individual gain, timing, and offset mismatches has been extensively discussed in the literature [1], [3], [10], [22], [25], [27]–[29]. This section gives more general description in terms of CTF. The TIADC linear model in Fig. 1(b) suggests each channel output is a *filtered* (by a CTF) and *aliased* (by an impulse train) version of the input spectrum. It can be shown that the kth channel output is written as

$$Y_k(f)=\frac{1}{M}\sum_{m=0}^{M-1}e^{-j2\pi k\frac{m}{M}}X\left(f-\frac{m}{M}f_S\right)H_k\left(f-\frac{m}{M}f_S\right),\quad k=0,1,\ldots,M-1 \tag{1}$$

where $X(f)$ is the Fourier transform of the input signal $x(n)$, and $H_k(f)$ is the kth channel CTF. The first term with $m=0$ corresponds to a desired signal component, while terms with $m=1,2,\ldots,M-1$ are frequency-shifted versions of the

input spectrum. When all channel outputs are combined to yield a TIADC output $Y(f)$, these frequency-translated versions of the input spectrum are cancelled if all CTFs are the same. In the presence of CTF mismatches, however, cancellation is imperfect, producing aliasing error, as will be discussed below.

The final output of the four-channel $(M = 4)$ TIADC, $Y(f)$ in Fig. 1(b), is obtained by summing all channel outputs

$$Y(f) = \begin{pmatrix} c_0(f)X(f) \\ +c_1\left(f-\frac{1}{4}f_S\right)X\left(f-\frac{1}{4}f_S\right) \\ +c_2\left(f-\frac{2}{4}f_S\right)X\left(f-\frac{2}{4}f_S\right) \\ +c_3\left(f-\frac{3}{4}f_S\right)X\left(f-\frac{3}{4}f_S\right) \end{pmatrix} \quad (2)$$

where $c_m(\cdot)$'s are defined as

$$\begin{aligned} c_0(f) &= \frac{1}{4}\big(H_0(f)+H_1(f)+H_2(f)+H_3(f)\big) \\ c_1(f) &= \frac{1}{4}\big(H_0(f)-jH_1(f)-H_2(f)+jH_3(f)\big) \\ c_2(f) &= \frac{1}{4}\big(H_0(f)-H_1(f)+H_2(f)-H_3(f)\big) \\ c_3(f) &= \frac{1}{4}\big(H_0(f)+jH_1(f)-H_2(f)-jH_3(f)\big). \end{aligned} \quad (3)$$

Equation (2) shows the TIADC output spectrum generally has both the desired signal and a frequency-shifted aliasing component, each with a corresponding gain $c_m(f)$ defined in (3). $c_m(f)$ is an effective conversion gain from an input signal at f to a frequency-shifted output at $f + (m/M)f_S$. Throughout this paper, $c_0(f)$ will be referred to as *signal conversion gain*, while $c_{m\neq 0}(f)$ will be referred to as *noise conversion gain*. It is interesting to note from (3) that the set of conversion gain $\{c_0(f), c_1(f), \ldots, c_3(f)\}$ can be regarded as a four-point discrete Fourier transform (DFT) of the CTF sequence $\{H_0(f), H_1(f), \ldots, H_3(f)\}$. If all CTFs are the same (i.e., no mismatch), then all DFT coefficients, except $c_0(f)$, cancel, resulting in zero aliasing error. In this case, SFDR is, therefore, not limited by aliasing spurs. With the presence of channel mismatches, however, $c_{m\neq 0}(f)$ is nonzero, in general, and SFDR is limited by the aliasing spurs whose magnitude is proportional to the corresponding noise conversion gain $c_{m\neq 0}(f)$. Fig. 2 graphically illustrates how CTF mismatch generates spurious signals on the TIADC output spectrum.

It is noted in Fig. 2(b) that the positive and negative frequency components of the input spectrum each experiences different conversion gains. For example, assume a real-valued input sinusoid at f_{in}, which has two complex exponentials at frequencies f_{in} and $-f_{\text{in}}$ (or, equivalently, $-f_{\text{in}} + f_S$). The positive-frequency tone at f_{in} passes through the CTFs $\{H_0(f_{\text{in}}), H_1(f_{\text{in}}), \ldots, H_3(f_{\text{in}})\}$ and, by DFT analysis, we obtain the conversion gain $\{c_0(f_{\text{in}}), c_1(f_{\text{in}}), c_2(f_{\text{in}}), c_3(f_{\text{in}})\}$ with corresponding aliasing spurs at $\{f_{\text{in}}, f_{\text{in}} + (1/4)f_S, \ldots, f_{\text{in}} + (3/4)f_S\}$. On the other hand, the image tone at $-f_{\text{in}}$ experiences the channel gain $\{H_0(-f_{\text{in}}), H_1(-f_{\text{in}}), \ldots, H_3(-f_{\text{in}})\}$, which is equal to $\{H_0^*(f_{\text{in}}), H_1^*(f_{\text{in}}), \ldots, H_3^*(f_{\text{in}})\}$ ($(\cdot)^*$ denotes the complex conjugate). According to the properties of DFT [26], the resulting conversion gain is $\{c_0^*(f_{\text{in}}), c_3^*(f_{\text{in}}), c_2^*(f_{\text{in}}), c_1^*(f_{\text{in}})\}$ with output spurs at $\{-f_{\text{in}}, -f_{\text{in}} + (1/4)f_S, \ldots, -f_{\text{in}} + (3/4)f_S\}$.

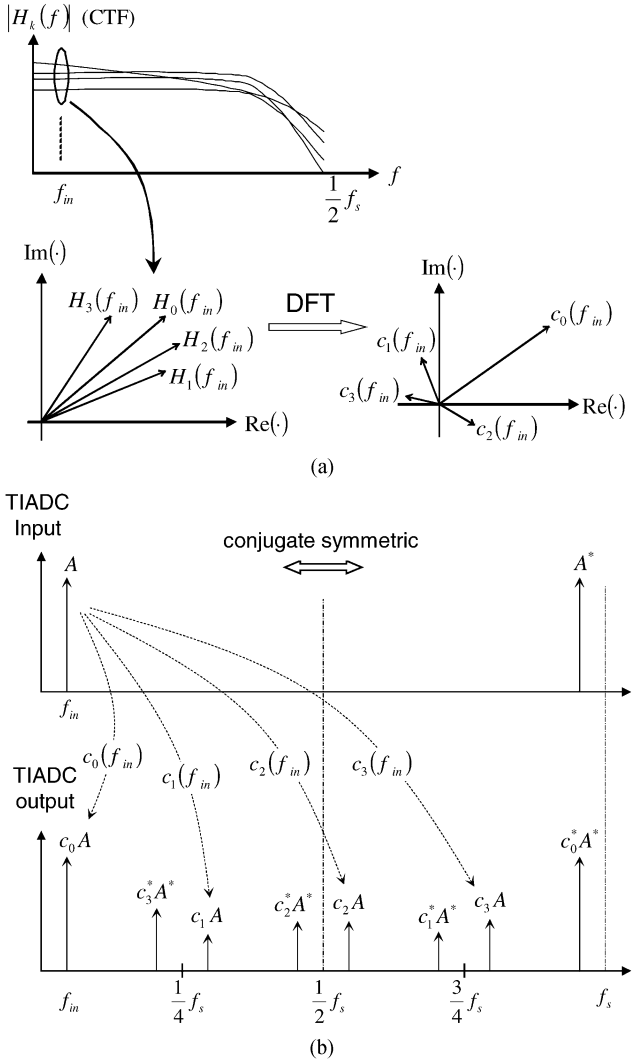

Fig. 2. Illustration of aliasing-spur generation mechanism. (a) In general, with channel mismatches, each CTF is a different function of frequency. CTFs and their DFT coefficients at f_{in} are plotted on a complex plane. It is seen that $c_{m\neq 0}(f_{\text{in}})$ are nonzero vectors due to the CTF mismatch at f_{in}. (b) Input and output spectrum with a real-valued sinusoid at f_{in}. The DFT coefficients of the CTF play the role of conversion gain from an input tone to each output spectral line including the signal tone, as well as aliasing spurs. Both input and output spectrum satisfies conjugate symmetry across dc and $f_S/2$. Note that spurious tones reduce the maximum SFDR achievable.

In summary, for an M-channel TIADC, with a real-valued input sinusoid at f_{in}, spurious tones due to the CTF mismatch are generated at

$$f_{\text{CTF error}} = \pm f_{\text{in}} + \frac{m}{M}f_S, \qquad m = 1, 2, \ldots, M-1. \quad (4)$$

On the other hand, the mismatch in channel dc offset produces error tones at the frequencies [29]

$$f_{\text{offset error}} = \frac{m}{M}f_S, \qquad m = 1, 2, \ldots, M-1. \quad (5)$$

It should be noted that offset mismatch does not modulate the input signal, but always produces spurs at fixed frequencies.

IV. Characterization of CTF

The CTF can be characterized at a single frequency by first applying a sinusoid with known frequency at the TIADC input, and then measuring the individual channel outputs. For a full characterization over a frequency range of interest, either a series of single-frequency tests must be performed or a carefully designed wide-band signal (e.g., a frequency-domain comb signal [22]) is required. Our work is based on a series of single-frequency measurements.

We assume a single sinusoid excitation. If we consider only the signal part (i.e., the output spectral line at the input frequency) from each channel output given by (1), then $Y_k(f) = (1/M)X(f)H_k(f)$. Hence, knowledge of the magnitude and phase of the input sinusoid allows unique determination of the value of the CTF at the input frequency. In order to identify the signal part, frequency-shifted spectra should not fall into the same frequency bin with the signal tone. It can be shown from (4) and (5) that the input signal frequency should satisfy $f_{\text{test}} \neq (m/2M)f_S$ and $f_{\text{test}} \neq (m/M)f_S$, where $m = 1, 2, \ldots, M-1$. These conditions can be met by a careful selection of test frequencies. For example, setting f_{test} to an integer multiple of $(1/P)f_S$, and making $2M$ and P relatively prime (i.e., have 1 as the only common factor) guarantees the signal tone is not ruined by mismatch spurs. In the case where the test signal generator has significant harmonic content, care has to be taken to avoid aliasing due to harmonics folded down to the first Nyquist zone. In some cases, bandpass filtering of the signal generator may provide enough attenuation. Alternatively, a certain set of calibration frequencies may be discarded. On the other hand, uncorrelated noise, such as phase noise, quantization noise, or wide-band white noise can be averaged out by taking a long acquisition time on the channel outputs.

The set of test frequencies should span at least the frequency range of interest (i.e., the passband of the input analog circuitry or the entire Nyquist zone if all-pass). The frequencies should be dense enough to accurately characterize channel mismatches. The value of CTF between measurement points, if needed in correction FIR filter design, may be estimated by interpolation [26]. It is noted, however, there is no practical substitute for an initial pilot characterization with a sufficiently large number of test frequencies. The number of test frequencies may be kept minimal once CTFs have been accurately characterized.

In practice, it is convenient to *normalize* a CTF with respect to an appropriately chosen reference (e.g., first-channel gain [22] or averaged CTF across channels). This is more practical than characterizing input sinusoids using an external amplitude and phase reference. Linear gain and phase distortion information, which is common to all channels in this case, may be lost during normalization. However, channel mismatch information, which is crucial to the SFDR performance of TIADC and, hence, also to the correction FIR filter design, is still preserved.

It is noted that a band-limited impulse may also be used for the purpose of CTF characterization. In general, however, a high-quality impulse is harder to generate, has a lower signal-to-noise ratio at a given peak voltage, and is more prone to aliasing than sinusoids due to its wide-band spectrum unless the antialiasing filter has a very sharp cutoff.

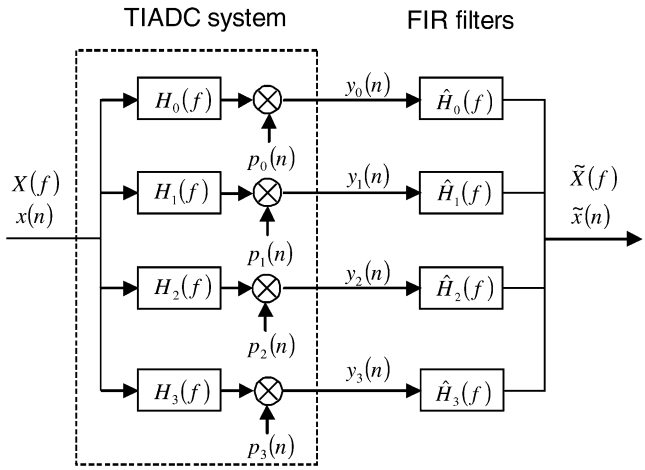

Fig. 3. TIADC cascaded by a set of mismatch-correction FIR filters.

V. Design of Correction FIR Filters

Once CTFs are measured, digital filters can be designed to correct mismatch errors. In Fig. 3, a length-N FIR filter is cascaded for every channel, and the filter outputs are then combined to form $\tilde{X}(f)$, the error-corrected output. Our goal is to make $\tilde{X}(f)$ a faithfully reconstructed version of the input $X(f)$. For an M-channel TIADC, $\tilde{X}(f)$ can be written, similarly as in (2), as a weighted sum of frequency-shifted input signal spectrum

$$\tilde{X}(f) = \sum_{m=0}^{M-1} \tilde{c}_m\left(f - \frac{m}{M}f_S\right) X\left(f - \frac{m}{M}f_S\right). \tag{6}$$

The conversion gain after correction ($\tilde{c}_m(f)$) is now a function of FIR filter coefficients as follows:

$$\begin{aligned}\tilde{c}_m(f) &= \frac{1}{M}\sum_{k=0}^{M-1} e^{-j2\pi k\frac{m}{M}} H_k(f)\hat{H}_k\left(f + \frac{m}{M}f_S\right) \\ &= \frac{1}{M}\sum_{k=0}^{M-1}\sum_{n=0}^{N-1} e^{-j2\pi k\frac{m}{M}} e^{-j2\pi n\left(\frac{f}{f_S}+\frac{m}{M}\right)} H_k(f)\hat{h}_k(n), \\ &\qquad m = 0, 1, \ldots, M-1.\end{aligned} \tag{7}$$

In (7), $\hat{h}_k(n)$ and $\hat{H}_k(f)$ are the impulse and frequency response of the kth channel length-N FIR filter, respectively. For *perfect reconstruction* of the input signal, $\hat{h}_k(n)$ needs to be designed so that $\tilde{c}_0(f)$ and $\tilde{c}_{m\neq 0}(f)$ are as close to an ideal time-delay system and zero as possible, respectively. For *aliasing-free reconstruction*, on the other hand, the only strict requirement is to make $\tilde{c}_{m\neq 0}(f)$ zero across the entire frequency range. In this case, $\tilde{c}_0(f)$ may introduce additional linear distortion as well as time delay. Mismatch spurs are still suppressed, however, and the spectral purity is not compromised by them. Therefore, both reconstruction strategies are equally effective in achieving a high SFDR as long as the linear distortion due to $\tilde{c}_0(f)$ is tolerable. In certain TIADC applications, where subsequent digital filtering is provided, the residual linear distortion can be further equalized.

There are MN unknown FIR filter coefficients, $\hat{h}_k(n)$'s, in (7), and these can be uniquely determined given a proper number of desired values of $\tilde{c}_m(f)$. One possible method is to solve the system of MN equations with an equal number

of unknowns by specifying the desired conversion gain for $m = 0, 1, \ldots, M-1$ over L discrete frequencies [22]–[24]. The proposed design approach based on WLS, however, fully exploits the stopband structure, thus, providing greater flexibility and a useful tradeoff in signal reconstruction.

A. WLS Formulation

We first form a system of conversion gain equations, for both signal and noise, by equating the right-hand side of (7) to a desired gain value over L discrete frequencies. With the incorporation of equation-wise weighting, the entire system of equations can be written in a standard matrix-vector form

$$\sqrt{\mathbf{W}}\mathbf{A}\hat{\mathbf{H}} = \sqrt{\mathbf{W}}\mathbf{D} \tag{8}$$

where each matrix or vector has a substructure as follows:

$$\mathbf{A} = \begin{pmatrix} \mathbf{a_{0,0}} & \mathbf{a_{0,1}} & \cdots & \mathbf{a_{0,M-1}} \\ \mathbf{a_{1,0}} & \mathbf{a_{1,1}} & & \mathbf{a_{1,M-1}} \\ \vdots & & \ddots & \vdots \\ \mathbf{a_{M-1,0}} & \mathbf{a_{M-1,1}} & \cdots & \mathbf{a_{M-1,M-1}} \end{pmatrix}$$

$$\sqrt{\mathbf{W}} = \begin{pmatrix} \sqrt{\mathbf{w_0}} & \mathbf{0} & \cdots & \mathbf{0} \\ \mathbf{0} & \sqrt{\mathbf{w_1}} & & \mathbf{0} \\ \vdots & & \ddots & \vdots \\ \mathbf{0} & \mathbf{0} & \cdots & \sqrt{\mathbf{w_{M-1}}} \end{pmatrix}$$

$$\hat{\mathbf{H}} = \begin{pmatrix} \hat{\mathbf{h}}_\mathbf{0} \\ \hat{\mathbf{h}}_\mathbf{1} \\ \vdots \\ \hat{\mathbf{h}}_\mathbf{M-1} \end{pmatrix}$$

$$\mathbf{D} = \begin{pmatrix} \mathbf{d_0} \\ \mathbf{0} \\ \vdots \\ \mathbf{0} \end{pmatrix} \tag{9}$$

where

$$\sqrt{\mathbf{w_m}} = \mathrm{diag}\left(\sqrt{w_m(f_0)} \quad \sqrt{w_m(f_1)} \quad \cdots \quad \sqrt{w_m(f_{L-1})}\right)$$

$$[\mathbf{a_{m,k}}]_{l,n} = \frac{1}{M} e^{-j2\pi k \frac{m}{M}} e^{-j2\pi n\left(\frac{f_l}{f_S}+\frac{m}{M}\right)} H_k(f_l)$$

$$\left[\hat{\mathbf{h}}_\mathbf{k}\right]_{n,1} = \hat{h}_k(n)$$

$$[\mathbf{d_0}]_{l,1} = d(f_l),$$

$m, k = 0, 1, \ldots, M-1$ (M: the number of channels)

$l = 0, 1, \ldots, L-1$ (L: the number of evaluation frequencies)

$n = 0, 1, \ldots, N-1$ (N: FIR filter length).

In (8), $\mathbf{A}$ is an $LM \times NM$, $\sqrt{\mathbf{W}}$ is an $LM \times LM$, $\hat{\mathbf{H}}$ is an $NM \times 1$, and $\mathbf{D}$ is an $LM \times 1$ matrix or row vector. The weighting matrix is represented in a square-root form for convenience. The desired conversion gain is specified by $\mathbf{D}$ (specifically, $\mathbf{d_0}$ and $\mathbf{0}$ for signal and noise conversion gain, respectively). Each conversion gain is evaluated at L discrete frequencies from f_0 to f_{L-1}. The first L equations in (8) define the signal conversion gain, and the remaining $(M-1)L$ equations dictate the aliasing noise conversion gain. If $L > N$, which is true, in general, (8) is an overdetermined system of equations, and the unique solution in a least square sense is [30]

$$\hat{\mathbf{H}}_\mathbf{WLS} = (\mathbf{A^H W A})^{-1}\mathbf{A^H W D} \tag{10}$$

where $(\cdot)^\mathbf{H}$ denotes complex-conjugate transpose. It can be shown that $\hat{\mathbf{H}}_\mathbf{WLS}$ minimizes the *weighted* mean-squared error between the desired conversion gain $\mathbf{D}$ and actual conversion gain $\mathbf{A}\hat{\mathbf{H}}_\mathbf{WLS}$. If $\mathbf{d_0}$ and L test frequencies are chosen such that complex-conjugate symmetry is obeyed, $\hat{\mathbf{H}}_\mathbf{WLS}$, obtained by (10), will be real valued. Otherwise, if we explicitly constrain $\hat{\mathbf{H}}$ to be real valued, the optimum solution is $\hat{\mathbf{H}}_\mathbf{WLS} = (\mathbf{Re}(\mathbf{A^H W A}))^{-1}\mathbf{Re}(\mathbf{A^H W D})$. Two design options are of interest: unweighted and weighted design.

B. Unweighted Filter Design

In unweighted design, the weighting matrix $\mathbf{W}$ is an identity matrix so that no equation in (8) is weighted heavier or lighter than others. The only parameter that controls the quality of error correction is N, the FIR filter length. Due to the *Gibbs* phenomenon [26], [31], the conversion gains realized by the resulting FIR filters usually have significant ripples. Ripples in signal conversion gain have a minor effect on SFDR, but ripples in noise conversion gains directly reduce SFDR by generating excessive aliasing spurs, as experimental results will later show. Therefore, in order to remove such ripples, filter coefficients are multiplied by a window function. Unweighted design is simple to use, but lacks flexibility. The designed filter, if multiplied by a window, is not optimal in any sense.

C. Weighted Filter Design

Weighted design provides more control over mismatch correction, and allows full exploitation of "don't care" frequency bands. In a classical FIR filter design, a "don't care" band (or "transition" band) refers to a frequency region where no desired filtering response is specified [31]. For TIADC mismatch correction, there is another useful observation: *aliasing spurs are free to remain uncancelled within "don't care" bands*. This additional benefit from "don't care" bands has not been exploited before to the authors' knowledge. All these relaxed requirements are taken into account by assigning zero or very small weights to the corresponding gain equations in (8). The resulting set of equations achieves a smaller total mean-squared error with the same number of FIR filter taps, yielding more satisfactory error correction.

In general A/D conversion systems, a bandpass input signal conditioning circuit (e.g., a transformer) introduces both lower and upper cutoff frequencies (f_L and f_H), and we naturally have two "don't care" bands: one in a lower end (dc to f_L) and the other in a higher end (f_H to $f_S/2$). Even without bandpass input circuitry, sampling time mismatches justify the use of a higher-end "don't care" band. In correcting timing mismatches by using FIR filters, there always exists an upper end frequency band where the approximation error is relatively large [32]. Although this error can be made smaller by using more FIR filter taps, the upper-end band can be advantageously considered a "don't care" one as well.

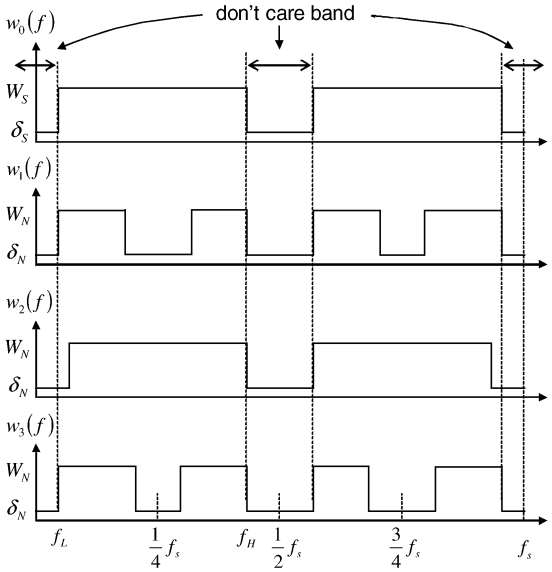

Fig. 4. Representative weighting scheme for a four-channel TIADC (i.e., illustration of (11) when $M = 4$). Input analog circuitry is assumed to have a passband from f_L to f_H. Corresponding stopbands are designated as "don't care," and, hence, have a very small weighting factor (δ_S or δ_N). Small-weight regions around $f_S/4$ correspond to input frequency bands where aliasing spurs fall into "don't care" bands.

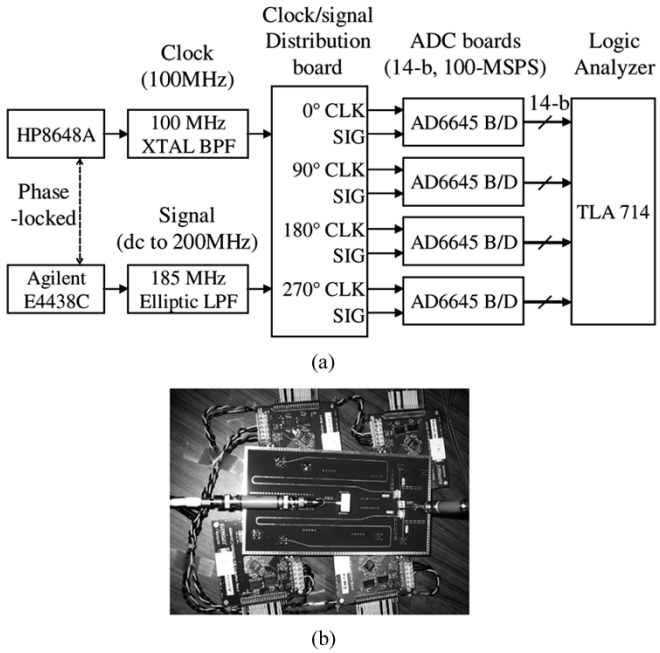

Fig. 5. Experimental setup for a 14-bit 400-MSPS TIADC prototype. (a) Block diagram. (b) Photograph of a clock/signal distribution board and four ADC boards.

We may also employ unequal weighting between signal and noise conversion gain equations for a tradeoff between the degree of aliasing-spur cancellation and the amount of residual linear gain-phase distortion. This realizes aliasing-free reconstruction (instead of perfect reconstruction) in a controllable manner.

With the incorporation of all previous considerations, weighting factors can be defined as (see Fig. 4 for a four-channel example)

$$w_0(f) = \begin{cases} \delta_S, & f \in \{\text{"don't care" band}\} \\ W_S, & \text{otherwise} \end{cases}$$

$$w_{m\neq 0}(f) = \begin{cases} \delta_N, & f \in \{\text{"don't care" band}\} \\ & \text{or } f + \dfrac{m}{M} f_S \in \{\text{"don't care" band}\} \\ W_N, & \text{otherwise,} \end{cases}$$

$$m = 0, 1, \ldots, M-1 \tag{11}$$

where $w_0(f)$ and $w_{m\neq 0}(f)$ quantifies the individual contribution of signal and noise conversion gain errors, respectively. It is understood that $W_S \gg \delta_S$ and $W_N \gg \delta_N$.

Weighting strategies for TIADC correction are summarized as follows.

1) Signal and noise conversion gain may be arbitrarily defined within "don't care" bands.
2) Aliasing spurs may fall into and remain uncancelled within "don't care" bands.
3) The amount of residual linear distortion can be traded off with the degree of aliasing-spur cancellation by adjusting W_N/W_S.

Applicability of each strategy may depend on the application. For example, 1) assumes input signal within the "don't care" bands is sufficiently weak or attenuated so that its aliasing spurs are negligible, and 2) and 3) implies subsequent digital filtering is capable of removing aliasing spurs within "don't care" bands or of equalizing the linear gain-phase distortion common to all channels.

VI. Experimental Results

To demonstrate the proposed calibration method, we developed, characterized, and performed mismatch correction on a four-channel TIADC prototype. 400 MSPS of aggregate sampling rate (f_S) is achieved with 14-bit resolution by interleaving four 14-bit 100-MSPS ADC chips [33]. Fig. 5 shows the experimental configuration. The clock and input test signal are phase locked to each other, and appropriately filtered to reject harmonics and wide-band white noise. A distribution board consists of power splitters and delay lines to provide four-phase 100-MHz clocks (i.e., 0°, 90°, 180°, and 270°) and an equal-phase input signal to the four ADC boards. The digital output is captured by a logic analyzer, and calibration is done on MATLAB. All instruments are controlled by custom software for automatic characterization.

A. Data Acquisition and CTF Characterization

For performance evaluation of the proposed correction method, data is acquired at 249 signal frequencies with $(1/500)f_S$ (=0.8 MHz) of spacing. The TIADC is first calibrated using every fourth frequency for CTF characterization: $(1/125)f_S, (2/125)f_S, \ldots, (62/125)f_S$. This particular choice of characterization frequencies systematically avoids aliasing due to mismatch spurs since 125 is relatively prime with $2M(=8)$. Although the signal generator's fourth harmonic falls into the same frequency bin as the fundamental tone at $(25/125)f_S$ and $(50/125)f_S$, the antialiasing filter [see Fig. 5(a)] attenuates the fourth harmonic to a negligible level. Channel offset is estimated by averaging the measured

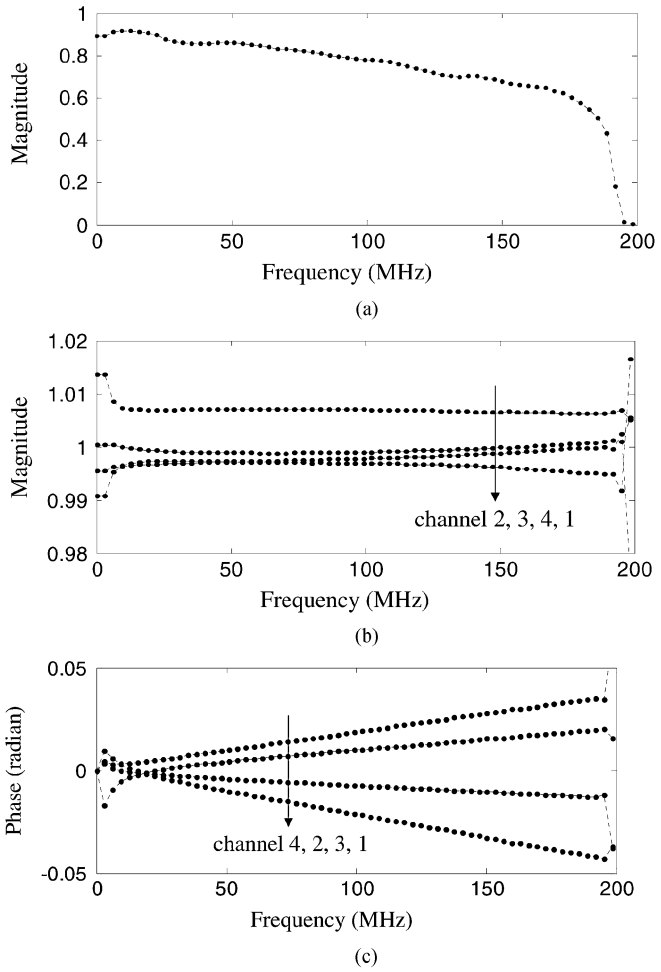

Fig. 6. Measured CTFs. (a) Average magnitude response before normalization. The antialiasing filter creates large attenuation over 185 MHz. Measured average phase response is not shown since the relative phase between the clock and signal is not known. (b) Magnitude and (c) phase response after normalization. Dots denote measurement points. The value of CTF at dc is set equal to the magnitude of nearest measured points (ADC boards have ac-coupled input circuitry).

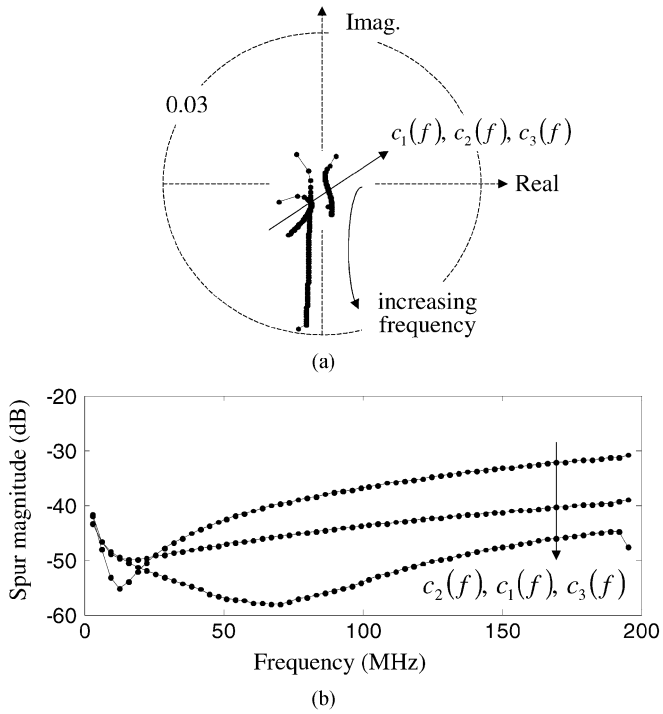

Fig. 7. (a) Polar and (b) decibel plot of noise conversion gains calculated from the measured CTFs in Fig. 6(b) and (c). $c_0(f)$ is always 1 due to the CTF normalization. Note that $c_2(f)$ is the dominant aliasing error except at low frequencies.

ADC dc output voltage for each run across the whole range of characterization frequencies.

Fig. 6(a) shows the average magnitude response of the measured CTFs (the output power variation with frequency arising from the signal generator is also lumped into the magnitude response). Fig. 6(b) and (c) shows the magnitude and phase response after normalization with respect to the average value across channels for each frequency. The relatively large mismatch at very low frequencies is due to differences between the low-frequency cutoffs of the ADC input transformers (which is approximately 2 MHz). The phase response at midband frequencies approximates a straight line, which suggests timing mismatch is dominant (approximately 1.3%, −0.6%, 0.4%, and −1.1% of the sampling period). The input antialiasing filter has approximately 50 dB of attenuation near 200 MHz. Random measurement error is, thus, amplified around this frequency, producing a large CTF mismatch near 200 MHz.

Fig. 7 shows noise conversion gains, which are calculated from DFT analysis of the normalized CTFs. Superposition of all three noise gains in a single decibel plot [see Fig. 7(b)] allows the prediction of uncalibrated SFDR performance to within the magnitude response of a normalization reference (i.e., average CTF values). It is seen in Fig. 7(a) and (b) that $c_2(f)$ creates the dominant aliasing spur ($\sim$−30 dB at high frequencies). $c_2(f)$ is the highest frequency component obtainable from four-point DFT, and its basis vector is an alternating sequence $\{1, -1, 1, -1\}$. This specific mismatch pattern can be traced back to the clock/signal distribution board where channel 1, 3 [two right ADC boards in Fig. 5(b)] and channel 2, 4 [two left ADC boards in Fig. 5(b)] each have identically shaped delay lines.

B. Mismatch Correction With Unweighted Filter Design

The previously estimated offset is subtracted from a corresponding channel output before dynamic mismatch correction. The FIR filter coefficients are first obtained by the unweighted least squares method, and then multiplied by a Hanning window to eliminate ripples in the frequency response. It has been found experimentally that 18 bit is sufficient for coefficient quantization with a reasonably small loss of performance (e.g., <1-dB SFDR loss). Fig. 8(a) and (b) shows the magnitude and phase response of the resulting 41-tap FIR filters. Dotted and solid lines each represent the frequency response before and after applying a Hanning window to the tap coefficients, respectively. It is seen that significant passband ripples are present before windowing, but they are smoothed out after windowing.

Fig. 9 shows a typical output spectrum before [see Fig. 9(a)] and after [see Fig. 9(b)] mismatch correction. The CTF and offset mismatch spurs (marked as X and O, respectively, in

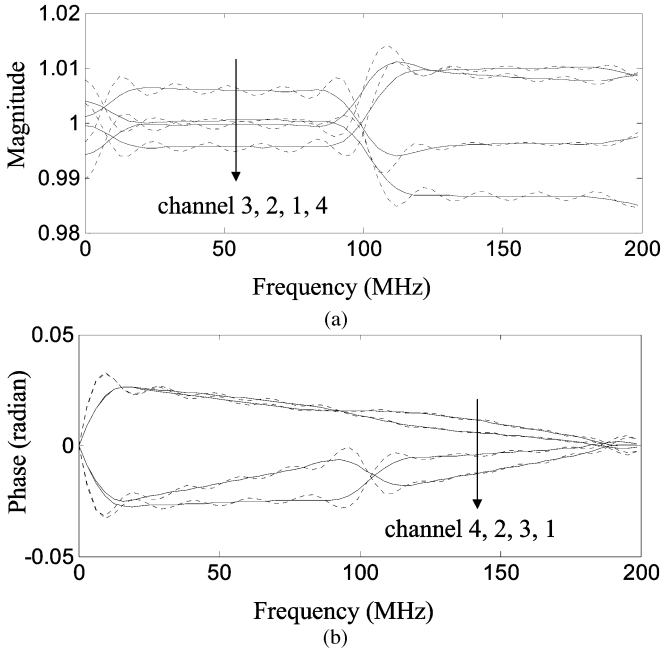

Fig. 8. (a) Magnitude and (b) phase responses of the correction FIR filters: unweighted design, 41 tap. The center tap is chosen as the time reference. Dotted and solid lines each represent the frequency response before and after applying a Hanning window to the tap coefficients.

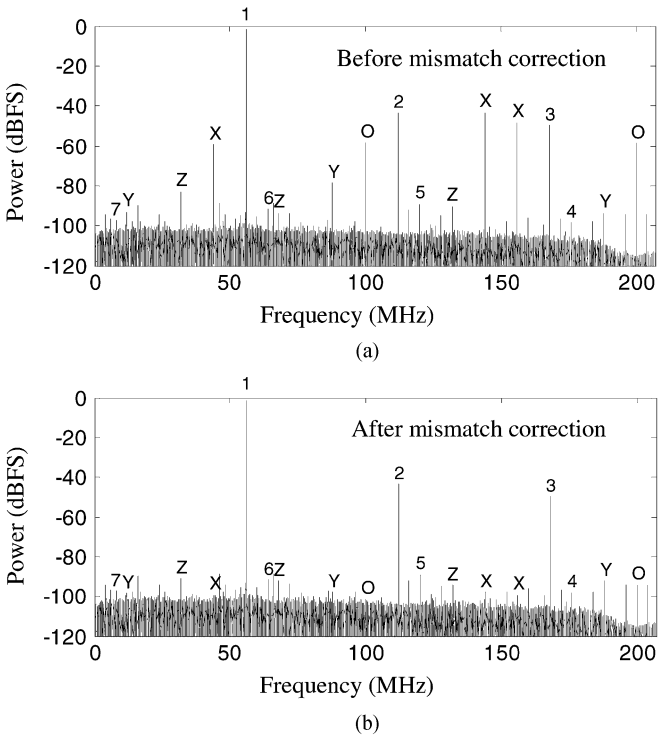

Fig. 9. Typical TIADC output spectrum (DFT of 62K samples): (a) before and (b) after mismatch correction by 21-tap FIR filters (unweighted design). An input sinusoid is applied at -1 dBFS and $(70/500)f_S$, which falls midway between two CTF characterization frequencies. Note that the noise floor reflects the antialiasing filter rolloff. The label 1 designates a fundamental tone, 2, 3, . . . , and 7 harmonics of the signal generator, X, Y, and Z CTF mismatch spurs due to the fundamental-, second-, and third-order harmonics, respectively, and the O offset mismatch spurs.

Fig. 9) are typically suppressed to better than 80 dB below full scale (dBFS). Low-order harmonics from the signal generator are seen to have a significant power level since they are within

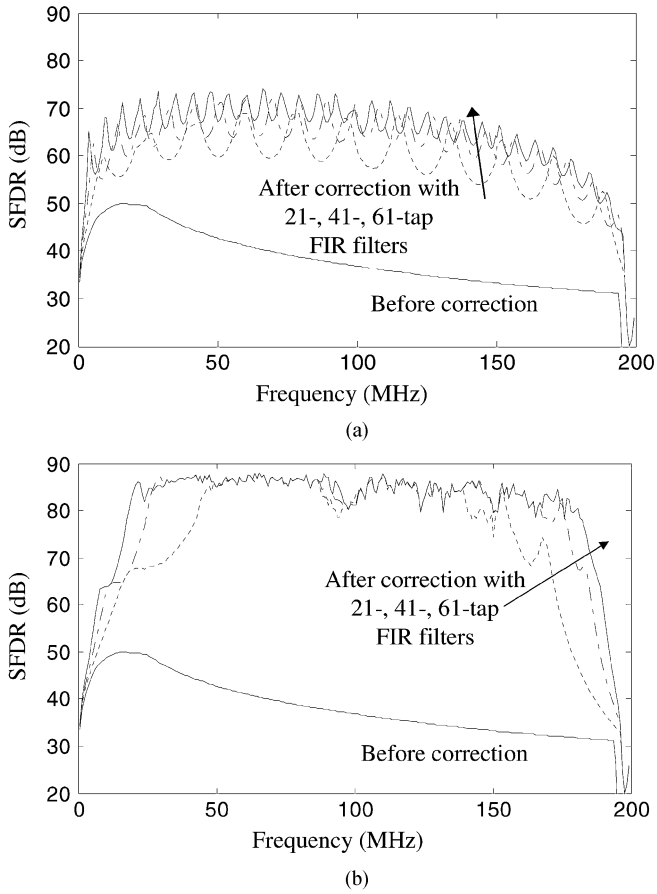

Fig. 10. Improvement in SFDR with mismatch correction: unweighted FIR design. (a) Before and (b) after applying a Hanning window to the FIR filter coefficients.

the passband of the antialiasing filter. It is noted that the signal generator harmonics, as well as a fundamental tone, generate corresponding aliasing spurs. The signal label, X, Y, and Z in Fig. 9 represent mismatch spurs at $\pm f_{\text{in}} + (m/M)f_S, \pm 2f_{\text{in}} + (m/M)f_S$, and $\pm 3f_{\text{in}} + (m/M)f_S$, respectively.

Fig. 10(a) and (b) shows the SFDR improvement over a full Nyquist zone by mismatch correction with FIR filters before [see Fig. 10(a)] and after [see Fig. 10(b)] windowing of filter coefficients. Signal generator harmonics up to seventh order are neglected for all SFDR measurements. The inferior SFDR characteristics seen in Fig. 10(a) compared to those of Fig. 10(b) is a direct result of excessive ripples in realized noise conversion gains, which are, in turn, due to the ripples in the frequency response of the unwindowed FIR filters. For the remainder of this paper, windowing of tap coefficients is assumed whenever an unweighted FIR design is discussed.

Before correction, the SFDR is limited by mismatch spurs over the entire Nyquist zone. After correction, the percentage of bandwidth where mismatch spurs determine SFDR is only 52%, 27%, and 22% for 21-, 41-, and 61-tap FIR filters, respectively, if we do not consider the upper and lower 20 MHz. For the rest of the frequency region, SFDR is typically limited by nonharmonic spurs at $f_{\text{in}} \pm 10$ MHz or higher order (>seventh) harmonics, both coming from the signal generator.

The SFDR drop at both ends of the Nyquist zone originates from phase discontinuities near dc and 200 MHz seen in

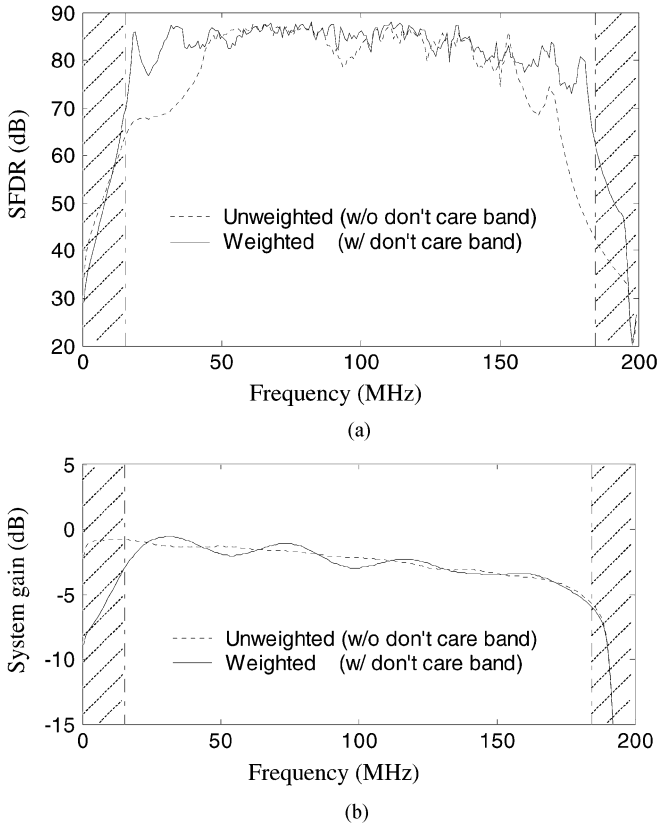

Fig. 11. Comparison of unweighted and weighted FIR filter design (21 tap). (a) SFDR performance after correction. (b) Overall system gain from TIADC input to corrected output. Shaded regions are "don't care" bands for weighted design.

Fig. 6(c). These discontinuities cannot be equalized by FIR filters and, therefore, approximation error is inevitably introduced. Windowing of the filter coefficients spreads this error in frequency [34] into a narrow frequency region if the FIR filter has many taps. Therefore, a longer FIR filter provides error correction over a wider range of frequencies. The sharp cutoff of antialiasing filter also contributes to a sudden SFDR drop near 200 MHz by quickly attenuating signal power.

The drop in SFDR at low frequencies may be eliminated by making the CTF phase continuous across dc (e.g., by using dc-coupled input analog circuitry or by sharing a single ac-coupled circuitry for all channels). In contrast, the drop in SFDR near $f_S/2$ cannot be completely removed due to the inherent phase discontinuity across the Nyquist frequency in the presence of timing mismatches. Using longer FIR filters, however, extends effective mismatch correction to higher frequencies.

Note the close agreement of uncalibrated SFDR between the measurement [see Fig. 10(a) or (b)] and prediction [see Fig. 7(b)].

C. Unweighted Versus Weighted Filter Design

Fig. 11 compares weighted and unweighted filter design. The FIR filters have 21 taps in both cases. The unweighted FIR filter design is the same as in Fig. 10(b). For the weighted design, "don't care" bands are set to the upper and lower 7.6% of Nyquist zone, where systematic SFDR drop occurs. We also choose W_N/W_S to be large in favor of strong cancellation of

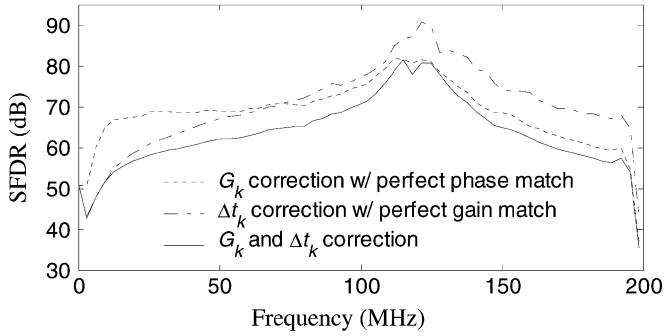

Fig. 12. Calculated SFDR with frequency-independent gain (G_k) and timing mismatch (Δt_k) correction (solid curve). Dotted and dashed–dotted line each represents the limiting SFDR after frequency-independent correction considering only gain and phase mismatch, respectively.

aliasing spurs rather than perfectly flat gain and phase response. Resulting weighting factors are $W_S = 1, W_N = 3 \cdot 10^5$, and $\delta_S = \delta_N = 0.001$. As seen in Fig. 11(a), the weighted design enables a wider frequency range of mismatch correction than the unweighted design with an equal number of FIR filter taps. Spurious signals within the "don't care" bands are ignored in the SFDR calculation for the weighted design. This improvement is obtained, however, by introducing some amount of linear gain-phase distortion into the overall system transfer function from TIADC analog input to corrected digital output. In Fig. 11(b), the dotted curve is the system gain realized with the unweighted FIR filter design, and is equal to the average CTF, which serves as a reference for CTF normalization. It is seen that the system gain with weighted filter design [solid line in Fig. 11(b)] has additional linear distortion (<2.5 dB) with respect to the reference. This distortion may be equalized by subsequent digital filtering if needed.

Although sinusoids are used for the SFDR performance test, it is noted that the proposed calibration method is equally effective with any band-limited input signal, as this can be represented as a sum of sinusoids within the Nyquist zone. This is because the TIADC system is linear and time-invariant once mismatches are corrected (this can be seen from (6) with $\tilde{c}_{m\neq 0}(f) = 0$).

D. Frequency-Dependent Versus Frequency-Independent Correction

Traditional frequency-independent calibration is compared with the proposed correction method. From the measured CTFs in Fig. 6(b) and (c), a best fit frequency-independent gain and timing error [G_k and Δt_k in Fig. 1(a)] are individually extracted for each channel. The upper and lower 20 MHz are not considered during the extraction for a better fit within the passband (20–180 MHz). A new set of CTFs are generated by directly calibrating out the errors, i.e., $H_k'(f) = H_k(f)/G_k e^{-j2\pi f \Delta t_k}$. The magnitude of aliasing spurs are predicted from noise conversion gains, which are obtained by DFT analysis, as discussed in Section III. The resulting SFDR is shown as a solid curve in Fig. 12, and is typically 10–25 dB worse than the one attained with the comprehensive correction in Figs. 10 and 11. Also shown in Fig. 12 are the maximum SFDR achievable after frequency-independent correction, limited by the residual gain (or phase) mismatch assuming no phase (or gain) mismatch.

E. System Drift

The TIADC prototype system was put into 4 h of continuous operation after a 1.5-h warm-up period. Data was acquired every half hour. Correction FIR filters were designed using the first acquisition data, and SFDR performance was evaluated for every subsequent data. Calibration accuracy ($\sim$80 dB of SFDR) was maintained up to the third acquisition (1-h operation). The loss of SFDR after 4 h was approximately 10–15 dB. We expect that the drift rate may be much less with a monolithic implementation, where thermal gradients and PC-boards and cable phase shifts are minimized. These important considerations are still under investigation and will be reported in the future.

VII. Conclusion

Digital correction of frequency-dependent mismatch error is essential for high-resolution and high-speed TIADCs. In this paper, we have proposed and demonstrated a comprehensive correction method, which is capable of exploiting stopband structure. Although we have assumed linearity, actual ADCs may exhibit significant nonlinearity. For example, we find experimentally that the CTF is a weak function of input signal amplitude. For a high-resolution converter, even a slight calibration detuning may result in a significant loss of SFDR.

Further research is required to address secondary effects not considered in this paper such as nonlinearity, temperature effect, aging, component drift, etc.

Acknowledgment

The authors would like to thank Prof. K. T. Cheng, Electrical and Computer Engineering (ECE) Department, University of California at Santa Barbara (UCSB), for the use of the TLA 714 Tektronix logic analyzer. The authors appreciate the helpful comments of Prof. S. Chandrasekaran, ECE Department, UCSB. The authors would also like to thank various comments from anonymous reviewers, which helped to make this paper more consistent.

References

[1] W. C. Black, Jr. and D. A. Hodges, "Time interleaved converter arrays," *IEEE J. Solid-State Circuits*, vol. SSC-15, no. 6, pp. 1022–1029, Dec. 1980.

[2] K. Poulton, J. J. Corcoran, and T. Hornak, "A 1-GHz 6-bit ADC system," *IEEE J. Solid-State Circuits*, vol. SSC-22, no. 6, pp. 962–970, Dec. 1987.

[3] A. Montijo and K. Rush, "Accuracy in interleaved ADC systems," *Hewlett-Packard J.*, vol. 44, no. 5, pp. 38–46, Oct. 1993.

[4] T. R. Clark and P. J. Matthews, "Real-time photonic analog-digital converter based on discrete wavelength-time mapping," in *Int. Topical Microwave Photonics Meeting*, vol. 1, Nov. 1999, pp. 231–234.

[5] R. C. Williamson, P. W. Juodawlkis, J. L. Wasserman, G. E. Betts, and J. C. Twichell, "Effects of crosstalk in demultiplexers for photonic analog-to-digital converters," *J. Lightw. Technol.*, vol. 19, no. 2, pp. 230–236, Feb. 2001.

[6] J. C. Twichell, J. L. Wasserman, P. W. Juodawlkis, G. E. Betts, and R. C. Williamson, "High-linearity 208-MS/s photonic analog-to-digital converter using 1-to-4 optical time-division demultiplexers," *IEEE Photon. Technol. Lett.*, vol. 13, no. 7, pp. 714–716, Jul. 2001.

[7] P. W. Juodawlkis, J. C. Twichell, G. E. Betts, J. J. Hargreaves, R. D. Younger, J. L. Wasserman, F. J. O'Donnell, K. G. Ray, and R. C. Williamson, "Optically sampled analog-to-digital converters," *IEEE Trans. Microw. Theory Tech.*, vol. 49, no. 10, pp. 1840–1853, Oct. 2001.

[8] K. Poulton, R. Neff, A. Muto, W. Liu, A. Burstein, and M. Heshami, "A 4 GSample/s 8b ADC in 0.35 μm CMOS," in *Int. Solid-State Circuits Conf. Tech. Dig.*, vol. 1, Feb. 2002, pp. 166–457.

[9] K. Poulton, R. Neff, B. Setterberg, B. Wuppermann, T. Kopley, R. Jewett, J. Pernillo, C. Tan, and A. Montijo, "A 20 GS/s 8b ADC with a 1 MB memory in 0.18 μm CMOS," in *Int. Solid-State Circuits Tech. Dig.*, 2003, pp. 318–319.

[10] Y. C. Jenq, "Digital spectra of nonuniformly sampled signals: Fundamentals and high-speed waveform digitizers," *IEEE Trans. Instrum. Meas.*, vol. 37, no. 3, pp. 245–251, Jun. 1988.

[11] ——, "Digital spectra of nonuniformly sampled signals: A robust sampling time offset estimation algorithm for ultra high-speed waveform digitizers using interleaving," *IEEE Trans. Instrum. Meas.*, vol. 39, no. 1, pp. 71–75, Feb. 1990.

[12] C. S. G. Conroy, D. W. Clind, and P. R. Gray, "An 8-b 85-MS/s parallel pipeline A/D converter in 1-μm CMOS," *IEEE J. Solid-State Circuits*, vol. 28, no. 4, pp. 447–454, Apr. 1993.

[13] K. C. Dyer, D. Fu, S. H. Lewis, and P. J. Hurst, "An analog background calibration technique for time-interleaved analog-to-digital converters," *IEEE J. Solid-State Circuits*, vol. SC-33, no. 12, pp. 1912–1919, Dec. 1998.

[14] D. M. Hummels, J. J. McDonald II, and F. H. Irons, "Distortion compensation for time-interleaved analog to digital converters," in *Proc. IEEE Instrumentation Measurement Technology Conf.*, vol. 1, Jun. 1996, pp. 728–731.

[15] Y. C. Jenq, "Perfect reconstruction of digital spectrum from nonuniformly sampled signals," *IEEE Trans. Instrum. Meas.*, vol. 46, no. 3, pp. 649–652, Jun. 1997.

[16] D. Fu, K. C. Dyer, S. H. Lewis, and P. J. Hurst, "A digital background calibration technique for time-interleaved analog-to-digital converters," *IEEE J. Solid-State Circuits*, vol. SC-33, no. 12, pp. 1904–1911, Dec. 1998.

[17] H. Jin and K. F. Lee, "A digital-background calibration technique for minimizing timing-error effects in time-interleaved ADC's," *IEEE Trans. Circuits Syst. II, Analog Digit. Signal Process.*, vol. 47, no. 7, pp. 603–613, Jul. 2000.

[18] S. M. Jamal, D. Fu, N. C. J. Chang, P. J. Hurst, and S. H. Lewis, "A 10-b 120-Msample/s time-interleaved analog-to-digital converter with digital background calibration," *IEEE J. Solid-State Circuits*, vol. SC-37, no. 12, pp. 1618–1627, Dec. 2002.

[19] W. Namgoong, "Finite-length synthesis filters for nonuniformly time-interleaved analog-to-digital converter," in *Proc. IEEE Int. Circuits Systems Symp.*, vol. 4, May 2002, pp. 815–818.

[20] J. M. D. Pereira, P. M. B. S. Girao, and A. M. C. Serra, "An FFT-based method to evaluate and compensate gain and offset errors of interleaved ADC systems," *IEEE Trans. Instrum. Meas.*, vol. 53, no. 2, pp. 423–430, Apr. 2004.

[21] A. Petraglia and S. K. Mitra, "High-speed A/D conversion incorporating QMF bank," *IEEE Trans. Instrum. Meas.*, vol. 41, no. 3, pp. 427–431, Oct. 1992.

[22] S. R. Velazquez, "Hybrid filter banks for analog/digital conversion," Ph.D. dissertation, Dept. Elect. Eng. Comput. Sci., MIT, Cambridge, MA, 1997.

[23] S. R. Velazquez, T. Q. Nguyen, and S. R. Broadstone, "Design of hybrid filter banks for analog/digital conversion," *IEEE Trans. Signal Process.*, vol. 46, no. 4, pp. 956–967, Apr. 1998.

[24] S. R. Velazquez and R. J. Velazquez, "Parallel processing analog and digital converter," U.S. Patent 6 473 013, Oct. 29, 2002.

[25] P. Löwenborg, "Asymmetric filter banks for mitigation of mismatch errors in high-speed analog-to-digital converters," Ph.D. dissertation 787, Dept. Elect. Eng., Linköping Univ., Linköping, Sweden, Dec. 2002.

[26] S. K. Mitra, *Digital Signal Processing: A Computer-Based Approach*. New York: McGraw-Hill, 2001.

[27] A. Petraglia and S. K. Mitra, "Analysis of mismatch effects among A/D converters in a time-interleaved waveform digitizer," *IEEE Trans. Instrum. Meas.*, vol. 40, no. 10, pp. 831–835, Oct. 1991.

[28] B. Yu and W. C. Black, Jr., "Error analysis for time-interleaved analog channels," in *Proc. IEEE Int. Circuits Systems Symp.*, vol. 1, May 2001, pp. 468–471.

[29] N. Kurosawa, H. Kobayashi, K. Maruyama, H. Sugawara, and K. Kobayashi, "Explicit analysis of channel mismatch effects in time-interleaved ADC systems," *IEEE Trans. Circuits Syst. I, Reg. Papers*, vol. 48, no. 3, pp. 261–271, Mar. 2001.

[30] T. K. Moon and W. C. Stirling, *Mathematical Methods and Algorithms for Signal Processing*. Upper Saddle River, NJ: Prentice-Hall, 2000.

[31] T. W. Parks and C. S. Burrus, *Digital Filter Design*. New York: Wiley, 1987.

[32] V. Välimäki, "Discrete-time modeling of acoustic tubes using fractional delay filters," Ph.D. dissertation, Dept. Elect. Commun. Eng., Helsinki Univ. Technol., Helsinki, Finland, 1995.
[33] "AD6645: 14-Bit, 80/105 MSPS A/D converter data sheet," Analog Devices Inc., Norwood, MA, 2003. [Online]. Available: http://www.analog.com.
[34] A. V. Oppenheim and R. W. Schafer, *Discrete-Time Signal Processing*. Englewood Cliffs, NJ: Prentice-Hall, 1989.
[35] "AD12400: 12-Bit, 400 MSPS A/D converter data sheet," Analog Devices Inc., Norwood, MA, 2004. [Online]. Available: http://www.analog.com.
[36] "AD12500: 12-Bit, 500 MSPS A/D converter data sheet," Analog Devices Inc., Norwood, MA, 2003. [Online]. Available: http://www.analog.com.

Munkyo Seo received the B.S.E.E. and M.S.E.E. degrees in electronic engineering from Seoul National University, Seoul, Korea, in 1994 and 1996, respectively, and is currently working toward the Ph.D. degree in electrical engineering at the University of California at Santa Barbara.

From 1997 to 2002, he was a Research Engineer with LG Electronics Inc., where he designed RF and microwave subsystems for wireless communication. His research interest includes microwave and mixed-signal circuit design and digital signal processing.

Mark J. W. Rodwell (M'89–SM'99–F'03) received the B.S. degree from the University of Tennessee at Knoxville, in 1980, and the M.S. and Ph.D. degrees from Stanford University, Stanford, CA, in 1982 and 1988, respectively.

He is currently Professor and Director of the Compound Semiconductor Research Laboratories, University of California at Santa Barbara. From 1982 to 1984, he was with AT&T Bell Laboratories. His research focuses on very high-bandwidth bipolar transistors, high-speed bipolar IC design, and gigahertz mixed-signal ICs. His group has worked extensively in the area of GaAs Schottky-diode ICs for subpicosecond/millimeter-wave instrumentation.

Dr. Rodwell was the recipient of a 1989 National Science Foundation Presidential Young Investigator Award, and the 1997 IEEE Microwave Prize for his work on submillimeter-wave diode ICs.

Upamanyu Madhow (S'86–M'90–SM'96) received the Bachelor's degree in electrical engineering from the Indian Institute of Technology, Kanpur, India, in 1985, and the M.S. and Ph.D. degrees in electrical engineering from the University of Illinois at Urbana-Champaign, in 1987 and 1990, respectively.

From 1990 to 1991, he was a Visiting Assistant Professor with the University of Illinois at Urbana-Champaign. From 1991 to 1994, he was a Research Scientist with Bell Communications Research, Morristown, NJ. From 1994 to 1999, he was with the Department of Electrical and Computer Engineering, University of Illinois at Urbana-Champaign, initially as an Assistant Professor and, since 1998, as an Associate Professor. Since December 1999, he has been with the Department of Electrical and Computer Engineering, University of California at Santa Barbara, where he is currently a Professor. His research interests are in communication systems and networking, with a current emphasis on wireless communication.

Dr. Madhow has served as associate editor for Spread Spectrum for the IEEE TRANSACTIONS ON COMMUNICATIONS and as associate editor for Detection and Estimation for the IEEE TRANSACTIONS ON INFORMATION THEORY. He was a recipient of the National Science Foundation (NSF) CAREER Award.